Rheumatol Int
DOI 10.1007/s00296-014-3052-9

REVIEW ARTICLE

Non-invasive and in vivo assessment of osteoarthritic articular cartilage: a review on MRI investigations

Ahmad Fadzil Mohd Hani · Dileep Kumar · Aamir Saeed Malik · Raja Mohd Kamil Raja Ahmad · Ruslan Razak · Azman Kiflie

Received: 24 February 2014 / Accepted: 16 May 2014

Abstract Early detection of knee osteoarthritis (OA) is of great interest to orthopaedic surgeons, rheumatologists, radiologists, and researchers because it would allow physicians to provide patients with treatments and advice to slow the onset or progression of the disease. Early detection can be achieved by identifying early changes in selected features of degenerative articular cartilage (AC) using non-invasive imaging modalities. Magnetic resonance imaging (MRI) is becoming the standard for assessment of OA. The aim of this paper was to review the influence of MRI on the selection, detection, and measurement of AC features associated with early OA. Our review of the literature indicates that the changes associated with early OA are in cartilage thickness, cartilage volume, cartilage water content, and proteoglycan content that can be accurately, consistently, and non-invasively measured using MRI. Choosing an MR pulse sequence that provides the capability to assess cartilage physiology and morphology in a single acquisition and advanced multi-nuclei MRI is desirable. The results of the review indicate that using an ultra-high magnetic strength, MR imager does not affect early OA detection. In conclusion, MRI is currently the most suitable modality for early detection of knee OA, and future research should focus on the quantitative evaluation of early OA features using advances in MR hardware, software, and data processing with sophisticated image/pattern recognition techniques.

Keywords Osteoarthritis · Articular cartilage · Magnetic resonance imaging · MR pulse · Multi-nuclei · Segmentation

A. F. M. Hani · D. Kumar (✉) · A. S. Malik
Department of Electrical and Electronic Engineering, Centre for Intelligent Signal and Imaging Research (CISIR), Universiti Teknologi PETRONAS, 31750 Tronoh, Perak, Malaysia
e-mail: dileep.kumar@petronas.com.my

A. F. M. Hani
e-mail: fadzmo@petronas.com.my

A. S. Malik
e-mail: aamir_saeed@petronas.com.my

R. M. K. R. Ahmad
Department of Electrical and Electronic Engineering, Universiti Putra Malaysia (UPM), 43400 Serdang, Selangor, Malaysia
e-mail: kamil@eng.upm.edu.my

R. Razak
Department of Orthopaedic, Pantai Hospital, Jalan Tambun, 31400 Ipoh, Perak, Malaysia
e-mail: rusraz55@gmail.com

A. Kiflie
Imaging Department, Pantai Hospital, Jalan Tambun, 31400 Ipoh, Perak, Malaysia
e-mail: azman_dr@yahoo.com

Introduction

Osteoarthritis (OA) is a joint disease characterized by the degeneration of the underlying articular cartilage (AC) tissue in any joint, though it commonly affects the knee [1, 2]. Early detection of OA, where changes to the affected knee components may still be reversible, is of great interest to orthopaedic surgeons, physicians, and researchers working in orthopaedics [3]. At the very least, early detection allows physicians to begin hyaluronic acid treatment, which can reduce the degeneration of articular cartilage [4], as well as dispense advice on weight control and lifestyle changes [5]. Physicians can also advise patients with a predisposition for OA to avoid performing activities involving excessive movement of the knee or taking up certain sports [6].

Published online: 31 May 2014

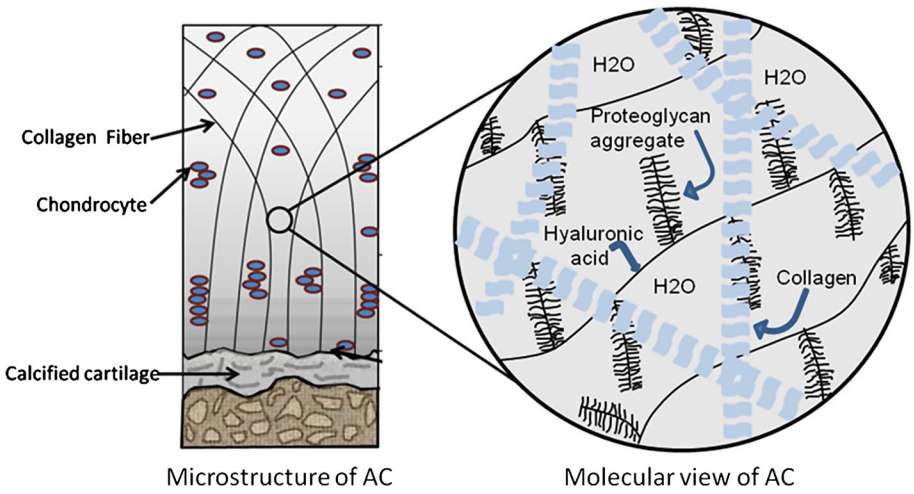

Fig. 1 Schematic representation of articular cartilage

The onset and progression of knee OA can be assessed by measuring changes associated with AC degeneration. AC is a fibrous tissue that is naturally stiff, yet deformable, which maintains the mechanical function of articulating bones. Smooth articulation of the joint depends on the AC composition and structure. AC is composed of water (60–80 %) and chondrocytes that are encased by extracellular matrix (ECM), as shown by schematic representation in Fig. 1. The ECM of AC is composed of type II collagen (5–10 %) and proteoglycans (PG) (10–20 %). All three components act together to provide the mechanical support (mechanical behaviour) necessary for smooth functioning of AC [7]. An imbalance in these molecular compositions results in cartilage abnormalities that lead to its degeneration. Structural (morphology) and molecular compositional (physiology) changes in articular cartilage have been used to detect and monitor the progression of OA at various stages using different modalities [8]. However, the successful measurement of morphological and physiological changes in certain features associated with AC degeneration depends on using an accurate, non-invasive, and high-resolution modality during the early stages of OA.

A number of non-imaging [quantitative ultrasound (QUS), vibro-arthrography (VAG), and electrical impedance plethysmography (EIP)] and imaging [X-ray, ultrasound, computed tomography (CT), nuclear imaging (scintigraphy), scanning acoustic microscopy (SAM), and magnetic resonance imaging (MRI)] have been used to assess various physiological and morphological changes associated with early degeneration of AC. MRI is often considered the most capable imaging modality because it allows the measurement of the structural and molecular contents of AC by means of images, providing quantitative information despite its non-invasive, non-ionizing, and in vivo nature [9, 10]. This paper provides an important perspective on the selection of several morphological and physiological features and grading systems that can be used to detect and monitor early knee OA non-invasively using MRI. In particular, features that change relatively rapidly and can be assessed by MRI are reviewed. An additional, in-depth discussion is included to demonstrate the suitability of MRI and influential MR parameters such as field strength, nuclei, and pulse sequences for the non-invasive detection of early OA in the following sections.

Selection of early knee OA features

The successful detection of early knee OA depends on the selection of features associated with AC degeneration that change relatively rapidly. Over the last two decades, the majority of research has focused on determining assessment features in three different categories: (1) features based on morphological measurements of AC, (2) features based on the mechanical and electrical properties of AC, and (3) features based on the molecular composition of AC. However, the detection of features that change rapidly is limited by the sensitivity of the imaging or non-imaging modality, its non-invasive nature, and the in vivo capabilities used for the assessment. The various features that have been used to detect OA at different stages of disease progression are summarized in Table 1.

The features listed in Table 1 have been measured using various imaging and non-imaging modalities that are summarized in Table 2 (morphological), Table 3 (biomechanical and bioelectrical), and Table 4 (physiological).

As shown in Tables 2, 3 and 4, MRI has been used to measure most of the features listed in Table 1. However, in all three categories, there are certain features that are more desirable to detect OA at an early stage.

Table 1 List of OA related features [7]

Morphological	Biomechanical/bioelectrical properties	Molecular composition
Joint width space	Biometric impedance	Water
Inflammation	Hydraulic permeability	Proteoglycans
Osteophytes	Fluid pressure	Collagen fibrillar network
Cartilage thickness	Electrokinetic phenomena	Collagen content
Cartilage surface area	Young's modulus/stiffness	
Cartilage volume		
Cartilage roughness		

Table 2 Modalities and morphological features of cartilage

Modality	Morphological features	References
X-ray	Joint width space, osteophytes	[11, 93, 94]
Computed tomography (CT)	Joint width space, osteophytes, cartilage surface area, cartilage integrity (quality), cartilage volume; cartilage roughness	[95–98]
Nuclear imaging (scintigraphy)	Joint width space, inflammation, osteophytes	[99–101]
Ultrasound	Inflammation, osteophytes, cartilage thickness, cartilage surface area, cartilage integrity (quality), cartilage roughness	[34, 102–104]
MRI	Joint width space, osteophytes, cartilage thickness, cartilage surface area, cartilage integrity (quality), cartilage volume, cartilage roughness	[20, 21, 28, 79, 84, 105–107]

Table 3 Modalities and biomechanical/bioelectrical properties of cartilage

Modality	Biomechanical/bioelectrical properties	References
Quantitative ultrasound (QUS)	Acoustic impedance young's modulus/stiffness	[17, 30, 34, 108]
Vibro-arthrography (VAG)	Vibration signal analysis	[18, 109, 110]
Electrical impedance plethysmography (EIP)	Bioelectric impedance	[31, 111]
Scanning acoustic microscope (SAM)	Acoustic impedance	[30, 112]
MRI (qMRI)	Hydraulic permeability Young's modulus/stiffness	[35, 36, 113]

Table 4 Modalities and molecular composition features of cartilage

Modality	Molecular composition features	References
Quantitative ultrasound (QUS)	Proteoglycan content	[16, 17, 34, 114]
	Collagen content	
	Collagen fibrillar network	
	Water content	
MRI (qMRI)	Proteoglycan content	[10, 16, 22, 40–42, 45–48, 59, 60, 62]
	Collagen content	
	Collagen fibrillar network	
	Water content	

Suitability of morphological features

Research studies have demonstrated that changes in certain morphological features (thickness, volume, and roughness) can be seen at OA grade 1 or 2, while other features such as joint width space and osteophytes show only minute changes in the early stages of OA and are thus indicative of severe OA grades [11–13]. A number of studies have reported that disturbances in the collagen fibrillar network of AC that result in increased cartilage surface roughness may be the first morphological features that can be measured [14, 15]. Changes in cartilage surface roughness can be detected using QUS indentation methods, which lead to better sensitivity and specificity in diagnosing OA at an early stage. However, QUS indentation methods are not recommended for clinical use because of their invasive nature;

Table 5 Correlation and accuracy in measuring thickness and volume of AC using MRI

Feature	Study	Validation method	Correlation	Accuracy/precision	Human/animal
Cartilage thickness	[27]	Needle probe	$r = 0.88$, $p < 0.0001$	MD (0.00 ± 0.23)	Bovine (in vitro)
	[28]	Direct measurement	$r = 0.92$	Accuracy-PD (±8.9 %)	Human (in vivo)
	[115]	Validated computerized algorithm	–	Precision-55 μm (mean lateral thickness)	Human (in vivo)
Cartilage volume	[29]	Directly measured volumes	$r = (0.90–0.98)$	Accuracy-PD (1.1–2.8 %)	Swine (in vitro)
	[85]	Semi-automated method	$r^2 > 0.91$	% Error-0.89 %	Human (in vivo)

MD mean difference, *PD* pairwise difference, *AD* average difference

they require an ultrasound probe to be in direct contact with extracted cartilage from the joint [16]. Although MRI has the capability to detect the fibrillation that forms roughness at the superficial articular surface, doing so remains challenging because the superficial surface of articular cartilage is only a few millimetres thick [17]. The knee joint vibration signal acquired using VAG is a useful indicator of cartilage surface roughness [18]. However, this method requires that the knee be in flexion during the VAG signal recording, which makes it uncomfortable, in particular for OA patients with severe pain, and is thus not suitable for clinical use.

Researchers have found that roughness of the AC surface causes changes in AC thickness and integrity (volume, area, and curvature) [19]. Therefore, studies on the morphology of AC are moving towards the measurement of cartilage thickness and volume over wide areas using non-invasive MRI [20–23]. The measurement of changes in cartilage thickness may provide an early indication of degeneration and can be used as morphological features to detect early OA. A decrease in the thickness of AC has been reported with the progression of OA. In a 3-week longitudinal study, the AC thickness was measured in the tibial cartilage from knee MR images of in vivo rat. Cartilage thickness decreased by 18 % at week 1 and 25 % at week 3 [24]. In another longitudinal study over a period of 36 months, cartilage thickness was evaluated from MR images of nine OA patients. The results showed a significant decrease of 0.85 % per year in the tibio femoral cartilage and 2.43 % per year in the femoral condyle cartilage [21]. In a third longitudinal study, a decrease in cartilage volume at the rate of ~5 % per year was observed in 123 OA patients [25]. A decrease of ~2.8 % in healthy cartilage has also been reported [26]. The studies measuring correlation, accuracy, and precision during volume and thickness measurement using MRI are shown in Table 5.

Based on Table 5, cartilage thickness measured using MRI on bovine cartilage has been validated against needle indentation with a significant correlation ($r = 0.88$, $p < 0.0001$) [27]. In this study, the accuracy of the method was determined by taking the mean difference between the thickness measured from MR images and an indentation method, and the results showed little difference in cartilage thickness (mean 0.00 ± 0.23 mm), indicating the accuracy of the measurement [27]. Very few studies have investigated the precision of MR cartilage thickness measurements, but one reported a precision in the range of 55 μm for minimum thickness to 77 μm for maximum thickness measurement on MR images [28]. For cartilage volume, the small pairwise difference (1.1–2.8 %) measured from the comparison of values derived from MR images to the values measured using direct measurement of the volume of extracted cartilage indicates the utility of MR images for volume computation [29]. Therefore, the measurement of morphological features associated with cartilage degeneration, including the volume and thickness of cartilage, can be measured successfully using MRI.

Suitability of biomechanical/bioelectrical features

Imbalances in the biochemical composition of AC lead to AC degeneration that can be evaluated through its electromechanical properties. Several of the electromechanical property-based features have been discussed previously [17, 30–33]. Similar to the morphology-based AC features, the changes in electromechanical property-based features vary at different stages of OA. Changes in certain features can be observed at the early degeneration stages, while others appear at later stages. At least one study has shown that the Young's modulus of AC reflects that the stiffness of cartilage during early OA [33] decreases, suggesting it is a suitable feature to assess early degeneration [33]. The several studies that have measured Young's modulus using MR analysis are listed in Table 6.

Values of Young's modulus measured using QUS show a positive and linear correlation ($r = 0.993$, $p < 0.05$) with values of dynamic modulus measured using mechanical indentation methods, with an approximate of 6.2 % error [34]. However, QUS involves the use of a mechanical testing device where the cartilage is compressed physically and requires the cartilage to be invasively dissected from joint. As depicted in Table 6, the studies that measure Young's

Table 6 Correlations between mechanical indentation and MR-based measurements of the dynamic Young's modulus of AC

Feature	Study	Validation method	Correlation	Accuracy/precision	Human/animal
Young's modulus	[36]	Mechanical indentation	$r = 0.681$	–	Bovine (in vitro)
	[35]	Mechanical indentation	$r^2 = 0.79$, $p < 0.001$	–	Bovine (in vitro)
	[16]	Mechanical indentation	$r = 0.50$, $p < 0.01$	–	Bovine (in vitro)

Table 7 Correlation between AC features and MR parameters

Feature	Study	Molecular content	Validation method	Correlation	Human/animal cartilage
Water	[47]	Water	Freeze-drying	$r = 0.885$, $p < 0.0001$	Rat (in vivo)
	[50]	Water	Freeze-drying	$r = 0.82$, $p < 0.01$	Bovine (in vitro)
Proteoglycan	[40]	PG	Spectrophotometer assay	$r = 0.85$, $p < 0.01$	Bovine (in vitro)
	[44]	PG	Dimethyl methylene blue (DMMB)	$r^2 = 0.8$	Bovine (in vitro)

modulus using MRI were conducted earlier and involve an indirect correlation of MR parameters with Young's modulus. MR techniques such as gadolinium-diethylenetriaminepentaacetic acid (Gd-DTPA^2) contrast enhancement imaging and corresponding $T1_{Gd}$ relaxation signals to calculate the negative fixed charge density (nFCD) of AC have been correlated with the dynamic Young's modulus of AC ($r^2 = 0.79$, $p < 0.001$ [35]; $r = 0.681$ [36]; and $r = 0.50$, $p < 0.01$ [16]), but do not yield good correlation. The measurement of Young's modulus as a feature of OA to assess changes during AC degeneration non-invasively has not yet proven effective, and further investigations are required.

Suitability of molecular composition (physiological) features

Because any changes occurring at the early stage of AC degeneration are due to an imbalance in biochemical composition, measuring this type of feature should also enable detection of early OA [33, 37]. At the very beginning, disruption of the collagen fibrillar network releases PGs, which influence the microstructural integrity of AC [38]. These disruptions can be visualized using scanning electron or confocal microscopy to identify microstructural changes in the cartilage [39], but these techniques are invasive by nature and require physical dissection of the AC. Any disturbance in the collagen fibrillar network of AC will lead to loss of PG content, which may further result in an increase in water content [14, 38]. A recent study reported that the significantly decreased PG content of the superficial zone of AC in the early stage of OA [38] can be measured using MRI [40–44]. Similarly, alterations in AC water content have been associated with early OA by several researchers [45–47]. The water content has been found to increase with increasing grades of OA [48, 49]. The studies estimating the correlation between MR parameters and AC molecular composition features are shown in Table 7.

The water and PG content of AC can usually be measured using QUS and qMRI. The QUS parameters such as reflection coefficient are associated with the water content of AC [34], as well as the PG content [16]. However, as indicated earlier, the QUS method requires the invasive dissection of cartilage from the joint. MRI is capable of assessing changes in the PG and water contents of AC that occur in the early stages of AC degeneration [10, 41, 42, 47, 50–52]. The water content of AC can be measured using MRI T1 and T2 relaxation parameters. Studies have reported a positive correlation between T1 relaxation ($r = 0.88$, $p < 0.0001$) and water content [47], as well as T2 relaxation ($r = 0.82$, $p < 0.01$) [50] with water content. In order to measure the PG content, hydrogen MR-based parameters such as T1ρ, delayed gadolinium-enhanced MRI of cartilage (dGEMRIC) (which requires intravenous injection of Gd-DTPA^{2-}), and sodium MRI have been used. A positive correlation was found between the T1ρ parameter and PG content ($r^2 = 0.80$) [44] and between sodium signals on sodium MR and PG content ($r = 0.85$, $p < 0.01$) [40]. For validation, the MR parameter values were compared with the absolute PG content of AC measured using freeze-drying and biochemical methods. Therefore, in order to assess the physiological changes associated with AC degeneration, water and PG are the most suitable parameters that can be accurately and non-invasively measured using MRI.

Based on the studies discussed above, the morphological features such as volume and thickness of AC and molecular composition features such as water and proteoglycan are the most desirable features that can be accurately and non-invasively measured using MR data to detect OA in the early stages. To increase the efficiency of early OA detection, measurement of more than one feature in combination is suggested.

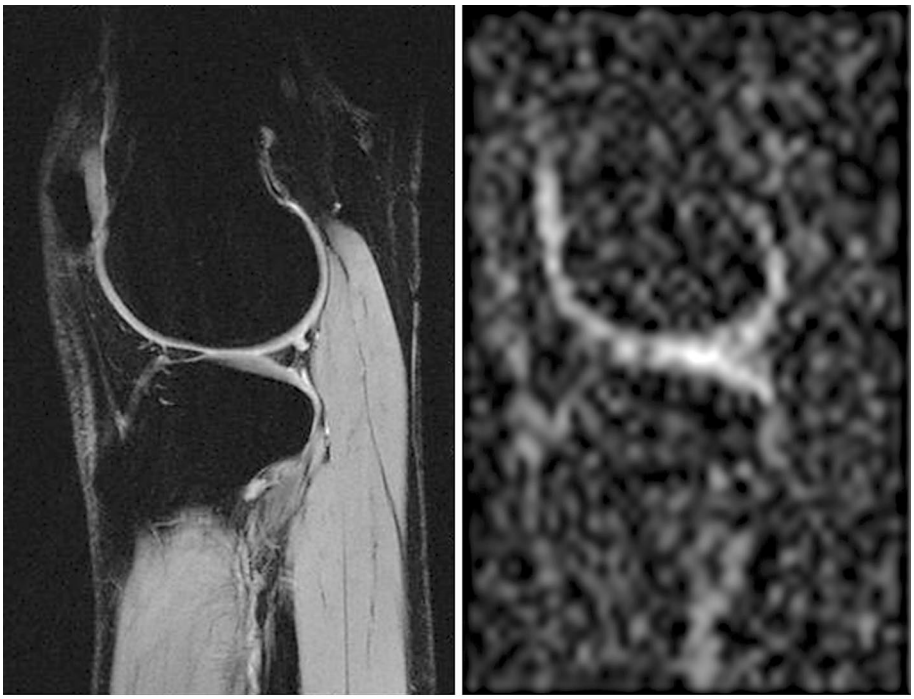

(a) (b)

Fig. 2 MR images of a knee acquired in vivo at 1.5 T. Hydrogen (^{1}H)-based (**a**) and sodium (^{23}Na)-based (**b**) MR images

Role of MRI for early OA detection

Magnetic resonance imaging (MRI) can assess the morphological and physiological properties of the tissues within the knee joint at different stages of OA progression. Eventually, changes during the preclinical stages of OA, where the symptomatic OA features are not yet known, may be detected by analysing MR data [53, 54]. MRI facilitates the measurement of changes in features that are useful for early OA detection and monitoring. One advantage of using the MR modality to measure early OA morphological features is that it provides better accuracy because of the excellent anatomical structure presented in the images. In particular, changes in the underlying physiology of degenerating AC can be measured using MRI to provide a quantitative assessment. However, the sensitivity of the measured morphological and physiological features using MRI is influenced by the choice of several contributing factors such as the selection of nuclei, magnetic field strength, and imaging sequence.

Selection of nuclei

The human body is composed of a large amount of water molecules. Therefore, hydrogen (^{1}H) nuclei-based MR scanning is performed in most clinical practices. MRI based on the localization of the different amounts of water molecules in body organs, which usually change due to any pathological disease conditions. In ^{1}H-based MR imaging, different amounts of water in an organ translates to the tissue contrast that provides the diagnostic capabilities for identifying the clinical changes between normal and diseased organs. However, ^{1}H is not the only nucleus used to perform MR scans; any nuclei that have an odd-numbered net spin such as phosphorus (^{31}P), sodium (^{23}Na), fluorine (^{19}F), and carbon (^{13}C) can be used [8, 43, 55–58]. Each of the nuclei used to perform MRI has its own advantages and suitability that depends on the body part to be scanned. For example, the composition of cartilage is rich in sodium, and one can acquire ^{23}Na nuclei-based MR images in order to extract more information about the knee joint along with ^{1}H-based MR images. An example of MR images acquired using hydrogen- and sodium-based nuclei of the same subject on at 1.5 T MR scanner is shown in Fig. 2.

The MR image based on sodium nuclei (Fig. 2b) provides high contrast in the sodium-rich cartilage region. However, several tissues are not visible, and where tissues are visible, their boundaries are somewhat blurred. The ^{1}H-based MR image shows several tissue types, but the contrast between the soft tissues, including the cartilage region, is low. In most cases, a nucleus other than ^{1}H is chosen based on the biochemical composition of the region of interest in a particular human organ and the amount of change in that nucleus during pathology. However, performing MR scanning using other nuclei requires the instalment of a specialized coil on the MR scanner that allows for excitation of the corresponding nucleus [58].

Hydrogen (^{1}H) nuclei-based MR scanning is used to assess morphological changes because it provides excellent anatomical detail of the synovial joint. Physical defects during OA progression can be detected from hydrogen-based MR images [9]. As discussed earlier, ^{1}H-based MR data are used to measure the volume and thickness of cartilage with high correlation (>0.90), minimal error (minimum of 0.89 %), and high precision (55 μm). Thus, for the measurement of the morphology of AC, ^{1}H-based MR imaging is suitable. However, this may not be true for the measurement of the physiological AC features. For cartilage physiological measurements, ^{1}H-based qMRI parameters such as T1, T2, T1ρ, and $T1_{Gd}$ relaxation times were found to be associated with the detection of early changes in the biochemical components [22, 32, 46, 50, 59].

The quantitative assessment of T1 and T2 MR relaxation times can be performed to measure increased water content of AC during early OA using ^{1}H-based MR data. The $T1_{Gd}$ relaxation time of ^{1}H MRI is associated with the PG content of AC. In this measurement, the Gd-DTPA^{2-} contrast enhancement agent is injected into the body before the MR scan. The measurement of $T1_{Gd}$ relaxation is time intensive [40, 60] and requires the acquisition of baseline signals prior to the addition of Gd-DTPA^{2-} [60]. Sodium (^{23}Na) MR imaging of AC, which is rich in sodium concentration, can supplement ^{1}H MR data, is non-invasive, and does not require a contrast agent. A direct measurement of PG depletion in degenerating AC can be made using sodium MRI because the loss of PG content results in a decreased concentration of sodium [48]. The PG content of AC maintains the fixed charge density (FCD) of the tissue through its negative charges. Sodium ions, on the other hand, are positively charged and are attracted to the FCD. Therefore, any changes in the negative FCD can be directly correlated to the changes in positive sodium ions [41, 42]. This relationship allows the loss of PG that is correlated to the loss of FCD [61] to be measured using sodium-based MRI. Therefore, many researchers are focusing on the measurement of PG content using sodium (^{23}Na)-based MRI [40, 41, 56, 57, 60, 62, 63].

Despite these advantages, sodium MRI remains difficult to apply because of the required field strengths (≥3 T) to obtain a significant signal-to-noise ratio (SNR, 12:1) and good anatomical images. In addition, sodium MRI requires a stronger gradient than ^{1}H-based MRI [64]. In order to overcome the problems associated with sodium MRI, one can use the advances in MR software and hardware. The development of radio-frequency (RF) coils and parallel imaging techniques such as sensitivity encoding (SENSE) [65] and simultaneous acquisition of spatial harmonics (SMASH) [66] allow for good resolution and high SNR at moderate (<3.0 T) field strengths on clinical sodium MR scanners. In addition, recent studies have reported that a direct measurement of sodium concentration, which is associated with changes in the PG content of AC, can be made with sodium MRI using a specialized radio-frequency (dual-tuned) coil [56–58]. Furthermore, a study using sodium MR on a 1.5 T MR scanner showed not only the applicability of the direct measurement of AC sodium concentration, but also the morphological measurement of AC [9]. To achieve this, MR data can be acquired using a dual-tuned knee coil without changing the position of the coil or the subject, and additional post-processing on the acquired data is performed using advanced image processing techniques that make the morphological measurement of AC feasible [67, 68].

Selection of MR pulse sequences

The choice of which MR pulse sequence to image cartilage tissue play a large role in the resulting image. In particular, it can increase the visibility of the cartilage, give better contrast in the cartilage compared to the surrounding tissues, and result in higher SNR and a faster scan time. Although a large numbers of sequences are available for cartilage imaging, they originate from two fundamental sequences: the spin echo (SE) and gradient echo (GRE) [55]. However, there are variants of each of these fundamental MR pulse sequences. In this review, we have summarized the commonly used MR pulse sequences for morphological imaging of cartilage as shown in Table 8.

In order to image cartilage morphology, most researchers have used the standard pulse sequences provided by the MR machine vendors. Standard 2D sequences include T1-weighted imaging, proton density (PD), and T2-weighted imaging with or without fat suppression. In addition, 3D spoiled gradient echo (SPGR) and fast low-angle shot (FLASH) sequences are also used to evaluate cartilage morphology [62]. Furthermore, in order to improve the visualization of cartilage pathology, additional fat suppression techniques are used in combination with the above-listed sequences [3]. High-resolution 2D images can be acquired using a traditional sequence with an acquisition time of about 2–3 min. Although 2D FSE/TSE images provide good results for detecting cartilage defects, they suffer from blurring and low contrast between tissues [69]. From Table 8, it can be seen that the 3D GRE sequence is best suited for morphological imaging within a reasonable scan time [70, 71].

Advances in pulse sequence development have demonstrated MRI's capability to provide morphological and biomechanical information on AC using a single-pulse sequence. The double-echo steady state (DESS) sequence has been reported as suitable for performing a single scan to measure cartilage anatomy because it produces

Table 8 Commonly used pulse sequences for cartilage imaging

Pulse sequence	Variants and abbreviations	Key features/achievements	Relation to early cartilage degeneration detection
Spin echo sequences	FSE	High-resolution 2D images	Excellent results in detecting cartilage defects
	TSE	Short scan time (2–5 min) [69]	
	MESE	MESE-scan time (about 10 min)	MESE best suited for T2 relaxation mapping (water content) [22, 72]
3D—GRE sequences	GRE/GRASS/FFE	High-resolution 3D images	Accurate cartilage thickness measurement [27, 70]
		Scan time (about 8 min 30 s) [56]	Depiction of structure is good
	SPGR/Flash/T1-FFE	Less SNR efficient[a]	Best suited for morphological imaging [71]
Multi-echo sequences	DESS	High-resolution 3D images	More sensitive to superficial lesions
		Suited for both morphology and physiologic assessment [71]	DESS provides universal cartilage discrimination [72]
			Bright signal on cartilage and synovial fluid
		Scan time (about 10 min) [98]	Technique not yet validated [71]
Driven equilibrium sequences	DEFT	Suffers from artefacts	Cartilage to fluid contrast is high
		Longer scan time (about 11 min)	Less fat suppression may lead to difficulties in cartilage thickness measurement [116]
		Choosing the right MR parameter is difficult	No blurring of high spatial frequencies
Steady-state sequences	bSSFP/TrueFISP/ FIESTA/bFFE	Produce 3D images	Off-resonance artefacts in imaging cartilage [8]
	FEMR	Shorter scan time (1–1.5 min) [69]	High contrast on cartilage for thickness measurement [69]
	FS-SSFP	Better SNR compared to FSE	
	LCSSFP	Transient artefacts	Less blurring and superior image contrast [69]

FSE f spin echo, *TSE* turbo spin echo, *MESE* multi-echo spin echo, *GRE* gradient recalled echo, *GRASS* gradient acquisition in the steady state, *FFE* fast field echo, *SPGR* spoiled gradient echo, *Flash* fast low-angle shot, *T1-FFE* T1-weighted fast field echo, *DESS* double-echo steady-state sequences, *DEFT* driven equilibrium Fourier transform, *SSFP* steady-state free precision, *bSSFP* balanced steady-state free precision, *TrueFISP* true fast imaging with steady-state precession, *FIESTA* fast imaging employing steady-state acquisition, *bFFE* balanced fast field echo, *FEMR* fluctuating equilibrium MR, *FS-SSFP* fat-saturated SSFP, *LCSSFP* linear combination SSFP [79]

[a] The ratio of SNR to the square root of total imaging time

high-resolution anatomical images and uses a different echo time to evaluate the T2 relaxation times. DESS also facilitates the acquisition of MR images in less scanning time with narrow slice thickness [71]. The osteoarthritis initiative (OAI) has developed protocols for knee imaging using MRI. They suggest that knee MR images acquired using the DESS sequence are able to provide universal discrimination of AC [72]. To date, the 3D SPGR and DESS sequences have been found to provide the best high spatial resolution images and anatomical structure visualization of cartilage. This is because the slice thickness and element size of the images influences the spatial resolution. Spatial resolution can be improved by decreasing the slice thickness during the acquisition, which is only possible with 3D volume acquisition [73]. The 3D SPGR and DESS sequences allow acquisition of slices with a thickness of <1 mm [74].

Advances in MR technology have made it possible to develop new sequences such as SSFP, FEMR, LCSSFP, and FS-SSFT, which were found to be more sensitive to the resonant frequency of certain tissue types [69]. Although advanced sequences such as SSFP, FEMR, LCSSFP, and FS-SSFT provide high contrast in cartilage with the shortest acquisition time, they suffer from artefacts that will make diagnosing OA at an early stage difficult. For the measurement of biochemical contents, such as water, that are associated with MR T2 relaxation times, the multi-echo spin echo (MESE) sequence with multiple echo times (used to measure the signal at different echo times from several slices) is the most suitable pulse sequence [22]. While the acquisition time for the MESE sequence is comparable to that of SPGR and DESS, detecting morphological changes in MESE images is challenging.

In general, the trend in MR sequencing is moving towards generating images with higher spatial resolution with shorter scan times. In the future, combined physiologic and morphologic information from AC should be targeted using a single-pulse sequence. To achieve this, the DESS sequence can be used to extract information on morphology and biochemical content (water only), but it has yet to be applied clinically [71]. In addition, future developments need to determine the pulse sequence that best provides data for assessing the morphological and physiological features associated with early degeneration of AC.

Selection of field of strength (Tesla)

Magnetic resonance imaging (MRI) field strengths can be generally categorized as low (<1.5 T), high (1.5–7.0 T), and ultra-high (>7.0 T) magnetic fields. Low-field MR scanners with conventional copper coils that operate at 0.18–0.20 T are not adequate to provide high-resolution MR images for good pathological visualization of cartilage [3]. Recent developments in MRI hardware have shown that high-temperature superconductor (HTS) coils operating in low-field MRI scanners (<0.5 T) provide better SNR compared to copper coils [75]. However, HTS coils were only tested by imaging human hands in vivo. Further study is required to assess their ability in knee cartilage imaging.

Many of the clinical MR systems for musculoskeletal imaging operate at 1.5 T field strength [3], but 3.0 T field strengths are commonly available and used in clinical practices. The trend in MRI research is moving towards the application of high and ultra-high magnetic field strengths that range from 3 to 9.4 T [59, 76–78]. Despite the high magnetic field, advanced pulse sequencing and RF coils in combination produce high spatial resolution images with a high SNR within a reasonable scan time. However, the acquired images are prone to an increase insusceptibility artefacts and chemical shift artefacts that could lead to inaccurate disease diagnoses [77]. A susceptibility artefact is caused by magnetic field inhomogeneity that results in irregular air-soft tissue interfaces, which can lead to misinterpretation [55]. Chemical shift artefacts result in dark and bright rims on opposite edges of the same tissue that are due to the movement of the frequency encoding in water and fat chemical environments.

Research results have not yet demonstrated any significant advantage of using high magnetic field strength (>1.5 T) to detect OA at an early stage. According to Kornaat et al. [79], the average thickness of cartilage measured from MR images acquired at 1.5 and 3.0 T result in similar values. This is because adequate segmentation of the cartilage was performed on the images acquired at 1.5 T despite the 3.0 T images having approximately twice the SNR and CNR efficiencies. This suggests that 1.5 T MR scanners provide sufficient spatial resolution and CNR to measure AC thickness. This measurement can be achieved by selecting a suitable imaging technique such as 3D SPGR or DESS. Similar to cartilage thickness, no significant difference in medial tibial or medial femoral cartilage volume was found when measured on a 1.5 and 3.0 T scanner under the effects of interference screws in a report by Bowers et al. [80].

One study on dynamic Young's modulus showed a moderate linear correlation with T2 relaxation times measured at 1.5 T ($r = -0.55$, $p < 0.01$) and 9.4 T ($r = -0.37$, $p < 0.01$) [78]. Lammentausta et al. also reported that even at lower field strength, the mean T2 relaxation values were larger than at higher field strengths, but the T2 variation with depth of the region of interest is independent of the field. This suggests that using a lower field (e.g. 1.5 T) magnet will result in similar T2 variation as higher field strength magnetic.

Lammentausta et al. [81] measured the T2 relaxation time of normal, moderate, and severe articular cartilage using 1.5 and 9.4 T fields. They found that the T2 relaxation times measured at 1.5 T were significant enough to demonstrate variations at normal to early and at advanced degeneration of AC. Conversely, no statically significant differences were found between the T2 relaxation times of all three groups at 9.4 T [81]. This further suggests that T2 relaxation times measured at 1.5 T provides better detection capabilities than operating at 9.4 T.

Another study measuring $T1_{Gd}$ relaxation time found no particular advantage in using 3.0 T MR compared to 1.5 T as the separation between the pre- and post-contrast relaxation rates was found to be less at 3.0 T compared with the results obtained at 1.5 T [82]. This is likely due to the lower contrast agent relativity at higher field strengths, suggesting that the $T1_{GD}$ variation at 1.5 T is sufficient to provide significant information on the PG content of AC in the early stages of OA. Considering the PG content measurement associated with sodium changes in AC, a 1.5 T scanner with advanced hardware capabilities was able to provide sodium MR data that could be processed to determine the sodium concentration of AC [57]. In a study conducted by Hani et al. [57], the sodium concentration measured from the analysis of sodium MR data acquired at 1.5 T matched the sodium concentration measured from the sodium MR data acquired at >3 T. Similarly, an optimal SNR in the cartilage region of sodium MR images obtained at 1.5 T also matched values reported from a >3 T MR scanner [58].

Knee MRI data processing

The physiology and morphology of AC can be measured during the early stages of disease progression using

Table 9 Automatic segmentation of articular cartilage from MRI images: sensitivity and specificity of existing methods

Method	Study	Validation method	Sensitivity (%)	Specificity (%)	Technique used
Automated articular cartilage segmentation	[117]	Manual	66.22	99.56	Region growing
	[86]	Manual	80.3	99.91	*k*NN classifiers
	[88]	Manual	83.7	99.9	3D active shape model
	[89]	Manual	83.9	99.9	Multi-class classification
	[90]	Manual	84.3	99.8	*k*NN classification
	[92]	Manual	93.8	99.3	Multiple MR sequence and support vector machine (SVM)
	[68]	Manual	80.27	99.65	Multinuclear MR and thresholding

quantitative measurement of selective features. It should be noted that highly skilled medical practitioners are able to use MR images for the interpretation of anatomical structure and diagnosis planning in OA. However, interpretation of the minute changes that occur during the early degeneration of OA is challenging because AC is only few millimetres thick has an irregular shape [20]. Research on assessing AC is moving towards the measurement of changes in different regions of AC because weight-bearing regions of cartilage are affected earlier than the non-weight-bearing regions [83]. Moving forward, cartilage changes during the early progression of disease will not only be distinguished by looking at different regions, but also at different layers of cartilage [22]. Studies have reported that the pattern of morphological change in different compartments of cartilage may be used with MRI to detect early OA by measuring a single-weight-bearing compartment [79]. MR parameters such as T2 relaxation time that are associated with the physiology of AC were found to be different in the deep and superficial layers of cartilage [22]. This suggests that for the accurate and consistent measurement of features associated with early OA, assessment of the different zones and compartments of AC should be performed. However, one of the challenging tasks in measuring cartilage morphology and physiology is in delineating the cartilage region in MR images from surrounding tissues using segmentation and visualization. As a result, a large number of studies have focused on applying advanced imaging and image processing techniques to segment AC on MR images [68, 70, 84–90].

Semi-automated AC segmentation methods are becoming important for assessing segmentation accuracy and consistency for the accurate diagnosis of disease. Most of the semi-automated methods rely on sophisticated image processing and analysis techniques to complete several steps automatically, followed by human user interactions to provide precision and accuracy. Although these methods are less time consuming than manual methods and provide more accurate results, for extensive studies in OA detection and monitoring that requires high consistencies over a long time, semi-automated methods are not suitable. In this review, automatic methods for AC segmentation on MR images are included as a suitable approach that is sensitive and feasible for application in clinical practices. A large number of studies have been conducted on automatically segmenting AC on MRI images. A few of these studies are summarized in Table 9, including their sensitivity and specificity, as well as the sophisticated image processing or pattern recognition techniques used.

Automatic segmentation of cartilage is performed on 2D, as well as on direct 3D, MR images. In general, the voxel classification methods use machine learning approaches such as the binary approximate k nearest neighbour (kNN) classifier to assign voxels as representing cartilage or the background [86]. The results from such classifications are then enhanced by applying a multivariant classifier that can extract voxels representing the cartilage region in MR images [87]. In these advanced methods, the classification of voxels was limited to the cartilage region only, and, in such cases, once a cartilage voxel is identified by the initial classifier, it will continue assigning all neighbouring cartilage voxels as such until reaching the last voxel [89]. In another method, multi-atlas registration is performed to segment the bone tissues, and then cartilage voxel likelihood probabilities are defined using the k nearest neighbour classifier [90]. Assuming that the voxel classification methods to segment articular cartilage on MR images are able to provide accurate and valuable results, the data set required for the training of the classifier algorithm for every change that happens to the imaging sequence is the main limitation to obtaining MR data.

Automatic segmentation of cartilage on MR images is an active field of research, and segmentation is being performed using several deformation models. Of these methods, active shape models are the most commonly used to segment AC on 3D MR images. Segmentation using active shape models involves two main steps: (1) the training of model parameters and (2) application of the model to a new data set [88]. The shape of the model to be applied can be generated by obtaining a set of corresponding control

points to form a similar shape. Once the shape model is ready, the shape is applied to a new image data set where each control point is assigned a probability of being in the cartilage region. Similar to classification-based methods, deformation methods require a training data set, which highlights their lack of flexibility for global use [88]. In addition, the methods mentioned above have not been tested in OA patients, where the changes in articular cartilage vary with the stage of disease.

Recently, advances in this field have been made in obtaining MR data using multiple-pulse sequences either in the same or in the different planes and performing the registration that is followed by segmentation. Most of the methods developed using multiple imaging sequences use two or more images acquired in the same plane. The registration is then performed to obtain the maximum amount of information available in both sequence images, resulting in more information on the cartilage and bone tissues that can be further used for automatic segmentation [91]. For example, by acquiring one sequence that is more sensitive to cartilage tissue contrast, another sequence that is more sensitive to bone, and registering both the images, the resultant would provide enhanced information on the cartilage and bone tissues that could further useful for automatic segmentation. In a recently developed method, three different contrast mechanisms were acquired and a feature vector consisting of different grey scale values in different contrast mechanisms was formed to classify the voxels representing the cartilage and non-cartilage regions [92]. That study reported a high sensitivity in cartilage segmentation. However, this method still requires training data sets to be prepared by manual methods. All the methods discussed above, except for the shape-based methods, use the pixel intensity values in an image. An automated method based on thresholding is the simplest way to segment when pixels having similar values are grouped together to form different regions in an image. Such methods are simple and fully automated, not requiring any user interaction. However, threshold-based methods are limited by the local variation in cartilage tissue properties that results in the following issues: (1) low contrast visibility in the cartilage region, (2) low signal intensities in the cartilage region compared with surrounding tissues, (3) variable intensities in different slices of a single data set, and (4) varying intensities in the cartilage region of a single slice. However, advances in image processing techniques have played a large role in overcoming the issues related to MRI of articular cartilage. Such advances may provide a better vision for overcoming the existing problems with MR images in order to develop a fully automatic articular cartilage segmentation method. Recent advances in MR hardware and software made it possible to obtain image data not only in different planes and using different imaging sequences, but also using multinuclear imaging facilities. Hani et al. [68] acquired sodium and proton MR knee images in the same plane, which were further used to perform fusion. The resulting fused images provided high contrast in the cartilage region and overcame several limitations of hydrogen-based knee MRI. Furthermore, automatic segmentation is performed on fused images by applying thresholding-based image processing techniques, which results in an adequate sensitivity and specificity.

In summary, the trend in measuring morphological and physiological changes in AC is moving towards assessing the different zones and compartments of AC, which requires advanced imaging and image processing techniques for the segmentation of AC on MR images. The developments of automatic articular cartilage segmentation methods are actively being researched, and the field remains open for discoveries, such as by applying advanced image or pattern recognition methods.

Conclusion

The onset and progression of knee OA can be assessed by measuring changes associated with AC degeneration. The majority of research that has been conducted to determine the features associated with early OA fall into three different measurement categories as listed in Table 1: (1) features based on the morphology of AC, (2) features based on the electromechanical properties of AC, and (3) features based on the molecular composition of AC. This review found that the features that undergo the earliest changes are surface roughness for morphology, cartilage stiffness for mechanical properties, and PG content for molecular composition. However, based on the studies reported above, the morphological features, such as AC volume and thickness, and molecular composition features, such as water and PG content, are the most desirable that can be accurately and non-invasively measured by using imaging modalities. To improve the efficiency of early OA detection, measurement of more than one feature in combination is suggested. The successful measurement of selected features associated with AC degeneration requires an accurate, non-invasive, and high-resolution modality to observe early AC degeneration. Currently, the evidence indicates that MRI is the most capable imaging modality to measure the structure and molecular contents of AC using images and quantitative information because of its non-invasive, non-ionizing, and in vivo nature. MRI is capable of acquiring the data needed to assess the physiological and morphological features of AC.

In order to measure the morphological features of cartilage thickness and volume, ^{1}H-based MR data analysis is adequate, and most studies report a high correlation,

minimal error, and significant precision when comparing results with ground truth measurements. However, this may not be true in the measurement of physiological AC features. For example, $T1_{Gd}$ relaxation times which are associated with PG's of AC provide significant accuracy. However, the $T1_{Gd}$ relaxation time of ^{1}H MRI requires injection of a contrast enhancement agent, which may not be feasible for all subjects. Alternatively, sodium concentration, which is associated with changes in PG content of AC, can be measured with sodium MR imaging that shows not only the applicability of the direct measurement of AC sodium concentration, but also the morphological measurement of AC. However, the combined measurement of physiology and morphology would require further advances in the development of MR hardware and pulse sequences. To this end, the DESS sequence can extract information on the morphology and biochemical content (water only) of AC and specialized hardware such as a dual-tuned knee coil can be used in combination. In general, the trend in MR pulse sequencing is moving towards generating images with higher spatial resolution in a shorter scan time. Future developments need to evaluate pulse sequences that can provide useful data for the morphological and physiological (sodium concentration) assessment of features associated with early degeneration of AC.

This review found that the trend in using MR scanners is moving towards high and ultra-high magnetic field strengths that have the capability to acquire high spatial resolution images with more significant SNR within a reasonable scan time. However, the high field strength MR scanners are susceptible to an increase in chemical shift artefacts that may lead to inaccurate diagnoses of disease. In addition, research results have not demonstrated any significant advantages to using high magnetic field strengths (>1.5 T) to detect OA at an early stage. High field strength (1.5 T) MR scanners with advanced imaging capabilities can provide MR data that could be further processed by applying sophisticated image and pattern recognition techniques for the early detection of OA. Currently, one of the challenges in MR data processing is the delineation of the cartilage region in MR images from the surrounding tissues by means of segmentation and visualization. The trend in segmentation of AC by applying advanced image and pattern recognition techniques is moving towards automatic methods that are capable of providing high sensitivity. This will enable the assessment of the morphology and physiology of degenerative changes in different AC zones and compartments. Automatic articular cartilage segmentation methods are still in development, and much remains to be discovered through the application of advanced image and pattern recognition methods.

In conclusion, a combination of multiple features associated with early OA, selective nuclei, a suitable MR pulse sequence, and advanced image and pattern recognition methods should improve current diagnostic capabilities for early OA detection. With this objective in mind, an MR-based clinical tool that incorporates a suitable pulse sequence, advanced hardware (such as a dual-tuned RF coil), and improved image data analysis will provide more direct information on the morphology and physiology of AC at the onset of OA.

Acknowledgments We would like to acknowledge Research and Innovation Office of Universiti Teknologi PETRONAS for their support as URIF Grant, Hospital Pantai, Ipoh, Malaysia, for their resources and Malaysian Government Science Fund Agency for E-science Fund (Grant No. 01-02-02-SF0150).

References

1. Lawrence RC, Felson DT, Helmick CG (2008) Estimates of the prevalence of arthritis and other rheumatic conditions in the United States. Part II. Arthritis Rheum 58(1):26–35
2. Quintana JM, Arostegui I, Escobar A, Azkarate J, Goenaga JI, Lafuente I (2008) Prevalence of knee and hip osteoarthritis and the appropriateness of joint replacement in an older population. Arch Intern Med 168(14):1576–1584
3. Link TM, Stahl R, Woertler K (2007) Cartilage imaging: motivation, techniques, current and future significance. Eur Radiol 17:1135–1146
4. Kaplan LD, Lu Y, Snitzer J et al (2009) The effect of early hyaluronic acid delivery on the development of an acute articular cartilage lesion in a sheep model. Am J Sports Med 37(12):2323–2327
5. Blagojevic M, Jinks C, Jeffery A, Jordan KP (2010) Risk factors for onset of osteoarthritis of the knee in older adults: a systematic review and meta-analysis. Osteoarthr Cartil 18:24–33
6. Spector TD, Harris PA, Hart DJ, Cicuttini FM, Nandra D, Etherington J, Wolman RL, Doyle DV (1996) Risk of osteoarthritis associated with long-term weight-bearing sports: a radiologic survey of the hips and knees in female ex-athletes and population controls. Arthritis Rheum 39(6):988–995
7. Hani AFM, Malik AS, Kumar D, Kamil R, Razak R, Kiflie A (2011) Features and modalities for assessing early knee osteoarthritis. In: International conference on electrical engineering and informatics (ICEEI), 17–19 July 2011, pp 1–6
8. Gold GE, Chen CA, Koo S, Hargreaves BA, Bangerter NK (2009) Recent advances in MRI of articular cartilage. AJR Am J Roentgenol 193(3):628–638
9. Hani AFM, Kumar D, Malik AS, Razak R, Kiflie A (2013) Fusion of multinuclear magnetic resonance images of knee for the assessment of articular cartilage. EMBC 2013. In: Annual international conference of the IEEE, 4–7 July, 2013, Osaka Japan, pp 6466–6469. doi:10.1109/EMBC.2013.6611035
10. Blumenkrantz G, Majumdar S (2007) Quantitative magnetic resonance imaging of articular cartilage. Eur Cells Mater 12:75–86
11. Felson DT, Gale DR, Elon Gale M, Niu J, Hunter DJ, Goggins J, LaValley MP (2005) Osteophytes and progression of knee osteoarthritis. Rheumatology 44:100–104
12. Guermazi A, Hunter DJ, Li L, Benichou O, Eckstein F, Kwoh CK, Nevitt M, Hayashi D (2012) Different thresholds for detecting osteophytes and joint space narrowing exist between the site investigators and the centralized reader in a multicenter

knee osteoarthritis study—data from the osteoarthritis initiative. Skelet Radiol 41(2):179–186
13. Teichtahl AJ, Wluka AE, Davies-Tuck ML, Cicuttini FM (2008) Imaging of knee osteoarthritis. Best Pract Res Clin Rheumatol 22(6):1061–1074
14. Hollander AP, Heathfield TF, Webber C, Iwata Y, Bourne R, Rorabeck C (1994) Increased damage to type II collagen in osteoarthritic articular cartilage detected by a new immunoassay. J Clin Invest 93:1722–1732
15. Hollander AP, Pidoux I, Reiner A, Rorabeck C, Bourne R, Poole AR (1995) Damage to type II collagen in aging and osteoarthritis starts at the articular surface, originates around chondrocytes, and extends into the cartilage with progressive degeneration. J Clin Invest 96:2859–2869
16. Kiviranta P, Töyräs J, Nieminen MT, Laasanen MS, Saarakkala S, Nissi MJ, Jurvelin JS (2007) Comparison of novel clinically applicable methodology for sensitive diagnostics of cartilage degeneration. Eur Cell Mater 13:46–55
17. Laasanen MS, Saarakkala S, Töyräs J, Hirvonen J, Rieppo J, Korhonen RK, Jurvelin JS (2003) Ultrasound indentation of bovine knee articular cartilage in situ. J Biomech 36:1259–1267
18. Rangaraj RM, Oloumi F, Wu Y, Cai S (2013) Fractal analysis of knee-joint vibroarthrographic signals via power spectral analysis. Biomed Signal Process Control 8(1):23–29
19. Montella A, Manunta A, Espa E, Gasparini G, De Santis E, Gulisano M (1992) Human articular cartilage in osteoarthrosis. I. The matrix. Transmission electron microscopic study. Ital J Anat Embryol 97(1):1–12
20. Mlejnek M, Vilanova A, Groller ME (2004) Interactive thickness visualization of articular cartilage. In: IEEE Visualization 10–15 Oct 2004, pp 521–527
21. Williams TG, Holmes AP, Bowes M, Vincent G, Hutchinson CE, Waterton JC, Maciewicz RA, Taylor CJ (2010) Measurement and visualisation of focal cartilage thickness change from MRI in a study of knee osteoarthritis using a novel image analysis tool. Br J Radiol 83(995):940–948
22. Carballido-Gamio J, Blumenkrantz G, Lynch JA, Link TM, Majumdar S (2010) Longitudinal analysis of MRI T2 knee cartilage laminar organization in a subset of patients from the osteoarthritis initiative. Magn Reson Med 63:465–472
23. Cromer MS, Bourne RM, Fransen M, Fulton R, Wang S-C (2013) Responsiveness of quantitative cartilage measures over one year in knee osteoarthritis: comparison of radiography and MRI assessments. J Magn Reson Imaging. doi:10.1002/jmri.24141
24. Xie Z, Liachenko S, Chiao P-C, Carvajal-Gonzalez S, Bove S, Bocan T (2010) In vivo MRI assessment of knee cartilage in the medial meniscal tear model of osteoarthritis in rats. In: Medical image computing and computer-assisted intervention—MICCAI 2010. Lecture notes in computer science, vol 6363, 57–64
25. Wluka AE, Stuckey S, Snaddon J, Cicuttini FM (2002) The determinants of change in tibial cartilage volume in osteoarthritic knees. Arthritis Rheum 46(8):2065–2072
26. Hanna F, Ebeling PR, Wang Y, O'Sullivan R, Davis S, Wluka AE, Cicuttini FM (2005) Factors influencing longitudinal change in knee cartilage volume measured from magnetic resonance imaging in healthy men. Ann Rheum Dis 64:1038–1042
27. Koff MF, le Chong R, Virtue P, Chen D, Wang X, Wright T, Potter HG (2010) Validation of cartilage thickness calculations using indentation analysis. J Biomech Eng 132(04):041007
28. Graichen H, Eisenhart-Rothe RV, Vogl T, Englmeier K-H, Eckstein F (2004) Quantitative assessment of cartilage status in osteoarthritis by quantitative magnetic resonance imaging: technical validation for use in analysis of cartilage volume and further morphologic parameters. Arthritis Rheum 50(3):811–816
29. Xing W, Sheng J, Chen WH, Tian JM, Zhang LR, Wang DQ (2011) Reproducibility and accuracy of quantitative assessment of articular cartilage volume measurements with 3.0 Tesla magnetic resonance imaging. Chin Med J (Engl) 124(8):1251–1257
30. Raum K (2008) Microelastic imaging of bone. Ultrason Ferroelect Freq Contr IEEE Trans 55:1417–1431
31. Gajre SS, Anand Sneh, Singh U, Saxena RK (2006) Novel method of using dynamic electrical impedance signals for non-invasive diagnosis of knee osteoarthritis. Conf Proc IEEE Eng Med Biol Soc 1:2207–2210
32. Perie D, Iatridis JC, Demers CN, Goswami T, Beaudoin G, Mwale F, Antoniou J (2006) Assessment of compressive modulus, hydraulic permeability and matrix content of trypsin-treated nucleus pulposus using quantitative MRI. J Biomech 39:1392–1400
33. Knecht S, Vanwanseele B, Stussi E (2006) A review on the mechanical quality of articular cartilage—implications for the diagnosis of osteoarthritis. Clin Biomech 21:999–1012
34. Saarakkala S, Laasanen MS et al (2003) Ultrasound indentation of normal and spontaneously degenerated bovine articular cartilage. Osteoarthr Cartil 11:697–705
35. Miyata S, Homma K, Numano T, Tateishi T, Ushida T (2010) Evaluation of negative fixed-charge density in tissue-engineered cartilage by quantitative MRI and relationship with biomechanical properties. J Biomech Eng 132(7):071014–071020
36. Nieminen MT, Töyräs J, Laasanen MS, Silvennoinen J, Helminen HJ, Jurvelin JS (2004) Prediction of biomechanical properties of articular cartilage with quantitative magnetic resonance imaging. J Biomech 37:321–328
37. Buckwalter JA, Mankin HJ (1998) Instructional course lectures, the American academy of orthopaedic surgeons—articular cartilage. Part II: degeneration and osteoarthrosis, repair, regeneration, and transplantation instructional course lecture. JBJA J Bone Joint Surg 79:4
38. Saarakkala SM, Julkunenz P, Kiviranta P, Mäkitalo J, Jurvelin JS, Korhonen RK (2010) Depth-wise progression of osteoarthritis in human articular cartilage: investigation of composition, structure and biomechanics. Osteoarthr Cartil 18:73–81
39. Wu JP, Kirk TB, Zheng MH (2008) Study of the collagen structure in the superficial zone and physiological state of articular cartilage using a 3D confocal imaging technique. J Orthop Surg Res 3:29
40. Borthakur A, Shapiro EM, Beers J, Kudchodkar S, Kneeland JB, Reddy R (2000) Sensitivity of MRI to proteoglycan depletion in cartilage: comparison of sodium and proton MRI. Osteoarthr Cartil 8:288–293
41. Wheaton AJ, Borthakur A, Shapiro EM, Regatte R, Akella SVS, Kneeland JB, Reddy R (2004) Proteoglycan loss in human knee cartilage: quantitation with sodium MR imaging—feasibility study. Radiology 231:900–905
42. Wheaton AJ, Dodge GR, Borthakur A, Kneeland JB, Schumacher R, Reddy R (2005) Detection of changes in articular cartilage proteoglycan by T1ρ magnetic resonance imaging. J Orthop Res 23(1):102–108
43. Bashir A (1995) Sodium NMR relaxation parameters in cartilage: implications for MR imaging. Ph.D. thesis, Massachusetts Institute of Technology
44. Duvvuri U, Kudchodkar S, Reddy R, Leigh JS (2002) T1ρ relaxation can assess longitudinal proteoglycan loss from articular cartilage in vitro. Osteoarthr Cartil 10:838–844
45. Lüsse S, Claassen H, Gehrke T, Hassenpflug J, Schunke M, Heller M, Gluer C-C (2000) Evaluation of water content by spatially resolved transverse relaxation times of human articular cartilage. Magn Reson Imaging 18:423–430

46. Liess C, Lusse S, Karger N, Heller M, Gluer C-C (2002) Detection of changes in cartilage water content using T2 mapping in vivo. Osteoarthr Cartil 10(12):907–913
47. Chou M-C, Tsai P-H, Huang G-S, Lee H-S, Lee C-H, Lin M-H, Lin C-Y, Chung H-W (2009) Correlation between the MR T2 value at 4.7 T and relative water content in articular cartilage in experimental osteoarthritis induced by ACL transaction. Osteoarthr Cartil 17:441–447
48. Shapiro EM, Borthakur A, Kaufman JH, Leigh JS, Reddy R (2001) Water distribution patterns inside bovine articular cartilage as visualized by 1H magnetic resonance imaging. Osteoarthr Cartil 9:533–538
49. Mankin HJ, Thrasher AZ (1975) Water content and binding in normal and osteoarthritic human cartilage. J Bone Joint Surg Am 57:76–80
50. Kurkijärvi JE, Nissi MJ, Rieppo J, Töyräs J, Kivirantad I, Nieminen MT, Jurvelin JS (2008) The zonal architecture of human articular cartilage described by T2 relaxation time in the presence of Gd-DTPA. Magn Reson Imaging 26:602–607
51. Kight AC, Dardzinski BJ, Laor T, Graham TB (2004) Magnetic resonance imaging evaluation of the effects of juvenile rheumatoid arthritis on distal femoral weight-bearing cartilage. Arthritis Rheum 50(3):901–905
52. Agarwal V, Kumar M, Singh JK, Rathore RKS, Misra R, Gupta RK (2009) Diffusion tensor anisotropy magnetic resonance imaging: a new tool to assess synovial inflammation. Rheumatology 48:378–382
53. Mechlenburg I, Nyengaard JR, Gelineck J, Soballe K (2007) Cartilage thickness in the hip joint measured by MRI and stereology e a methodological study. Osteoarthr Cartil 15:366–371
54. Davies M, Wluka AE, Wang Y, Teichtahl AJ, Jones G, Ding C, Cicuttini FM (2008) The natural history of cartilage defects in people with knee osteoarthritis. Osteoarthr Cartil 16:337–342
55. Bitar R, Leung G, Perng R et al (2006) MR pulse sequences: what every radiologist wants to know but is afraid to ask. Radiographics 26:513–526
56. Hani AM, Kumar D, Malik A, Walter N (2012) Non-invasive sodium MR imaging and quantification of in vivo articular cartilage at 1.5 Tesla. Osteoarthr Cartil 20(Supplement 1):S18–S19
57. Hani AFM, Kumar D, Malik AS, Razak R (2013) Physiological assessment of in vivo human knee articular cartilage using sodium MR imaging at 1.5 T. Magn Reson Imaging 31(7):1059–1067
58. Hani AFM, Kumar D, Malik AS (2012) Performance evaluation of dual tuned knee coil (^{23}Na/^{1}H) for articular cartilage imaging on 1.5 Tesla MRI. In: 4th International conference intelligence advanced system (ICIAS), vol 1, pp 357–361
59. Huang GS, Chou M-C, Shih Y-YI, Tsai P-H, Lin M-H, Lee C-H, Chung H-W (2010) Quantitative MR T2 measurement of articular cartilage to assess the treatment effect of intra-articular hyaluronic acid injection on experimental osteoarthritis induced by ACLX. Osteoarthr Cartil 18:54–60
60. Shapiro EM, Borthakur A, Gougoutas A, Reddy R (2002) ^{23}Na MRI accurately measures fixed charge density in articular cartilage. Magn Reson Med 47(2):284–291
61. Shapiro EM, Borthakur A, Dandora R, Kriss A, Leigh JS, Reddy R (2000) Sodium visibility and quantitation in intact bovine articular cartilage using high field ^{23}Na MRI and MRS. J Magn Reson 142:24–31
62. Gold GE, Burstein D, Dardzinski B, Lang P (2006) MRI of articular cartilage in OA: novel pulse sequences and compositional/functional markers. Osteoarthr Cartil 14:A76–A86
63. Bashir A, Gray ML, Hartke J, Burstein D (1999) Nondestructive imaging of human cartilage glycosaminoglycan concentration by MRI. Magn Reson Med 41(5):857–865
64. Borthakur A, Mellon E, Niyogi S, Witschey W, Kneeland JB, Reddy R (2006) Sodium and T1ρ MRI for molecular and diagnostic imaging of articular cartilage. NMR Biomed 19(7):781–821
65. Pruessmann KP, Weiger M, Scheidegger MB, Boesiger P (1999) SENSE: sensitivity encoding for fast MRI. Magn Reson Med 42(5):952–962
66. Sodickson DK, Manning WJ (1997) Simultaneous acquisition of spatial harmonics (SMASH): fast imaging with radiofrequency coil arrays. Magn Reson Med 38(4):591–603
67. Hani AM, Kumar D, Malik A, Razak R (2013) Accessibility to combined assessment of morphology and physiology in articular cartilage using ^{23}NA/^{1}H coil at 1.5 Tesla MRI. Osteoarthr Cartil 21(Suppl):S192–S193. doi:10.1016/j.joca.2013.02.405
68. Hani AM, Kumar D, Malik A, Walter N, Razak R, Kiflie A (2013) Automatic segmentation of articular cartilage from combined assessment of sodium and proton MR knee images. Osteoarthr Cartil 21(Suppl):S198–S199. doi:10.1016/j.joca.2013.02.416
69. Hargreaves BA, Gold GE, Beaulieu C, Vasanawala SS, Nishimura DG, Pauly JM (2003) Comparison of new sequences for high-resolution cartilage imaging. Magn Reson Med 49:700–709
70. Koo S, Gold GE, Andriacchi TP (2005) Considerations in measuring cartilage thickness using MRI: factors influencing reproducibility and accuracy. Osteoarthr Cartil 13:782–789
71. Eckstein F, Guermazi A, Frank W (2009) Quantitative MR imaging of cartilage and trabecular bone in osteoarthritis. Radial Clin N Am 47:655–673
72. Peterfy CG, Schneider E, Nevitt M (2008) The osteoarthritis initiative: report on the design rationale for the magnetic resonance imaging protocol for the knee. Osteoarthr Cartil 16(12):1433–1441
73. Loeuille D, Rat A-C, Goebel J-C, Champigneulle J, Blum A, Netter P, Gillet P, Chary-Valckenaere I (2009) Magnetic resonance imaging in osteoarthritis: which method best reflects synovial membrane inflammation? Correlations with clinical, macroscopic and microscopic features. Osteoarthr Cartil 17:1186–1192
74. Wirth W, Nevitt M et al (2010) Sensitivity to change of cartilage morphometry using Coronal FLASH, Sagittal DESS, and Coronal MPR DESS protocols—comparative data from the osteoarthritis initiative (OAI). Osteoarthr Cartil 18(4):547–554
75. Cheong H-S, Wild J, Alford N, Valkov I, Randell C, Paley M (2010) A high temperature superconducting imaging coil for low-field MRI. Concepts in magnetic resonance Part B. Magn Reson Eng 37(2):56–64
76. Taylor C, Carballido-Gamio J, Majumdar S, Li X (2009) Comparison of quantitative imaging of cartilage for osteoarthritis: T2, T1ρ, dGEMRIC, and contrast-enhanced CT. Magn Reson Imaging 27(6):779–784
77. Stahl R, Krug R, Kelley DA, Zuo J, Ma CB, Majumdar S, Link TM (2009) Assessment of cartilage-dedicated sequences at ultra-high-field MRI: comparison of imaging performance and diagnostic confidence between 3.0 and 7.0 T with respect to osteoarthritis-induced changes at the knee joint. Skelet Radiol 38:771–783
78. Lammentausta E, Kiviranta P, Nissi MJ, Laasanen MS, Kiviranta I, Nieminen MT, Jurvelin JS (2006) T2 relaxation time and delayed gadolinium-enhanced MRI of cartilage (dGEMRIC) of human patellar cartilage at 1.5 T and 9.4 T: relationships with tissue mechanical properties. J Orthop Res 24(3):366–374
79. Kornaat PR, Reeder SB, Koo S, Brittain JH, Yu H, Andriacchi TP, Gold GE (2005) MR imaging of articular cartilage at 1.5 T and 3.0 T: comparison of SPGR and SSFP sequences. Osteoarthr Cartil 13:338–344

80. Bowers ME, Tung GA, Trinh N et al (2008) Effects of ACL interference screws on articular cartilage volume and thickness measurements with 1.5 T and 3 T MRI. Osteoarthr Cartil 16:572–578
81. Lammentausta E, Kiviranta P, Töyräs J, Hyttinen MM (2007) Quantitative MRI of parallel changes of articular cartilage and underlying trabecular bone in degeneration. Osteoarthr Cartil 15:1149–1157
82. Williams A, Mikulis B, Krishnan N (2007) Suitability of T(1Gd) as the dGEMRIC index at 1.5 T and 3.0 T. Magn Reson Med 58(4):830–834
83. Karvonen RL, Negendank WG, Teitge RA, Reed AH, Miller PR, Fernandez-Madrid F (1994) Factors affecting articular cartilage thickness in osteoarthritis and aging. J Rheumatol 21(7):1310–1318
84. Carballido-Gamio J, Lee K, Ozhinsky E, Majumdar S (2004) MRI cartilage of the knee: segmentation, analysis, and visualization. In: Proceedings of international society of magnetic resonance medicine 11, 2004 (210)
85. Swamy MSM, Holi MS (2013) Knee joint articular cartilage segmentation using radial search method, visualization and quantification. Int J Biom Bioinform (IJBB) 7(1):1–13
86. Folkesson J, Olsen OF, Pettersen P, Dam E, Christiansen C (2005) Combining binary classifiers for automatic cartilage segmentation in knee MRI. In: ICCV 1st International workshop: computer vision for biomedical image applications, pp 230–239
87. Folkesson J, Dam E, Olsen OF, Pettersen P, Christiansen C (2005) Automatic segmentation of the articular cartilage in knee MRI using a hierarchical multi-class classification scheme. Med Image Comput Comput Assist Interv 8(Pt 1):327–334
88. Fripp J, Ourselin S, Warfield SK, Crozier S (2007) Automatic segmentation of the bones from MR images of the knee. In: Proceedings of IEEE 4th international symposium on biomedical imaging (ISBI-'07), Metro Washington, DC, USA, pp 336–339
89. Folkesson J, Dam EB, Olsen OF, Pettersen PC, Christiansen C (2007) Segmenting articular cartilage automatically using a voxel classification approach. IEEE Trans Med Imaging 26(1):106–115
90. Shan L, Charles C, Niethammer M (2012) Automatic multi-atlas-based cartilage segmentation from knee MR images. In: IEEE international symposium on biomedical imaging, pp 1028–1031
91. Tamez-Pena JG, Barbu-McInnis M, Totterman S (2004)Knee cartilage extraction and bone-cartilage interface analysis from 3-D MRI data sets. In: Proceedings of SPIE medical imaging 2004: image processing, vol 5370, pp 1774–1784
92. Koo S, Hargreaves BA, Andriacchi TP, Gold GE (2008) Automatic segmentation of articular cartilage from MRI: a multi-contrast and multi-dimensional approach. Proc Intl Soc Mag Reson Med 16:2546
93. Kijowski R, Blankenbaker D, Stanton P, Fine J, De Smet A (2006) Arthroscopic validation of radiographic grading scales of osteoarthritis of the tibiofemoral joint. AJR Am J Roentgenol 187:794–799
94. Neogi T, Niu J, Nevitt M, Lewis CE, Aliabadi P (2009) Association between radiographic features of knee osteoarthritis and pain: results from two cohort studies. BMJ 339:b2844
95. Onan OA, Hipp JA, Heggeness MH (1998) Use of computed tomography image processing for mapping of human cervical facet surface geometry. Med Eng Phys 20:77–81
96. Alvarez C, Chicheportiche V, Lequesne M, Vicaut E, Laredo J-D (2005) Contribution of helical computed tomography to the evaluation of early hip osteoarthritis: a study in 18 patients. Joint Bone Spine 72:578–584
97. Palmer AW, Guldberg RE, Levenston ME (2006) Analysis of cartilage matrix fixed charge density and three-dimensional morphology via contrast-enhanced microcomputed tomography. PNAS 103(51):19255–19260
98. Sniekers YH, Intema F, Lafeber FPJG, van Osch GJVM, van Leeuwen JPTM, Weinans H, Mastbergen SC (2008) A role for subchondral bone changes in the process of osteoarthritis; a micro-CT study of two canine models. BMC Musculoskelet Disord 9:20
99. Dieppe P, Cushnaghan J, Young P, Kirwan J (1993) Prediction of the progression of joint space narrowing in osteoarthritis of the knee by bone scintigraphy. Ann Rheum Dis 52:557–563
100. Appelboom T, Emery P, Tant L, Dumarey N, Schoutens A (2003) Evaluation of technetium-99m-ciprofloxacin (Infecton) for detecting sites of inflammation in arthritis. Rheumatology 42:1179–1182
101. Mazzuca SA, Brandt KD, Schauwecker DS, Buckwalter KA, Katz BP, Meyer JM, Lane KA (2004) Bone scintigraphy is not a better predictor of progression of knee osteoarthritis than Kellgren and Lawrence grade. J Rheumatol 31(2):329–332
102. Moller B, Bonel H, Rotzetter M, Villiger PM, Ziswiler HR (2009) Measuring finger joint cartilage by ultrasound as a promising alternative to conventional radiograph imaging. Arthritis Care Res 61(4):435–441
103. Spannow AH, Stenboeg E, Pfeiffer-Jensen M, Herlin T (2007) Ultrasound measurement of joint cartilage thickness in large and small joints in healthy children: a clinical pilot study assessing observer variability. Pediatr Rheumatol Online 5:3
104. Naredo E, Acebes C, Möller I et al (2009) Ultrasound validity in the measurement of knee cartilage thickness. Ann Rheum Dis 68(8):1322–1329
105. Agnesi F, Amrami KK, Frigo CA, Kaufman KR (2007) Semi-automated digital analysis of knee joint space width using MR images. Skelet Radiol 36:437–444
106. Kornaat PR, Bloem JL, Ceulemans RYT, Riyazi N, Rosendaal FR, Nelissen RG, Carter WO, Le Graverand M-PH, Kloppenburg M (2006) Osteoarthritis of the knee: association between clinical features and MR imaging findings. Radiology 239(3):811–817
107. Dam EB, Loog M, Christiansen C et al (2009) Identification of progressors in osteoarthritis by combining biochemical and MRI-based markers. Arthritis Res Ther 11:R115
108. Gelse K, Olk A, Eichhorn S, Swoboda B, Schoene M, Raum K (2010) Quantitative ultrasound biomicroscopy for the analysis of the healthy and repair cartilage tissue. Eur Cell Mater 19:58–71
109. Rangayyan RM, Wu Y (2010) Screening of knee-joint vibroarthrographic signals using probability density functions estimated with Parzen windows. Biomed Signal Process Control 5:53–58
110. Cai S, Yang S, Zheng F, Lu M, Wu Y, Krishnan S (2013) Knee joint vibration signal analysis with matching pursuit decomposition and dynamic weighted classifier fusion. Comput Math Methods Med 2013:904267. doi:10.1155/2013/904267
111. Neves EB, Pino AV, de Almeida RM, de Souza MN (2010) Knee bioelectric impedance assessment in healthy/with osteoarthritis subjects. Physiol Meas 31(2):207–219
112. Leicht S, Raum K (2008) Acoustic impedance changes in cartilage and subchondral bone due to primary arthrosis. Ultrasonics 48:613–620
113. Juras V, Bittsansky M, Majdisova Z, Szomolanyi P, Sulzbacher I, Gäbler S, Stampfl J, Schüller G, Trattnig S (2009) In vitro determination of biomechanical properties of human articular cartilage in osteoarthritis using multi-parametric MRI. J Magn Reson 197:40–47

114. Kuroki H, Nakagawa Y, Mori K, Kobayashi M, Yasura K, Okamoto Y, Suzuki T, Nishitani K, Nakamura T (2008) Ultrasound properties of articular cartilage in the tibio-femoral joint in knee osteoarthritis: relation to clinical assessment (International Cartilage Repair Society grade). Arthritis Res Ther 10(4):R78
115. Burgkart R, Glaser C, Hyhlik-Durr A, Englmeier K-H, Reiser M, Eckstein F (2001) Magnetic resonance imaging-based assessment of cartilage loss in severe osteoarthritis: accuracy, precision, and diagnostic value. Arthr Rheum 44(9):2072–2077
116. Link TM (2009) MR imaging in osteoarthritis: hardware, coils, and sequences. Radiol Clin N Am 47:617–632
117. Pakin SK, Tamez-Pena JG, Totterman S, Parker KJ (2002) Segmentation, surface extraction and thickness computation of articular cartilage. In: Proceedings of SPIE medical imaging 2002: image processing, vol 4684, pp 155–166